



Research on Pulsar Time Steered Atomic Time Algorithm Based on DPLL

Ze-Hao Zheng¹, Yang Liu², Dan Shen³, Fan Feng¹, Jiu-Long Liu¹, Yue-Xin Ma¹, and Xiang-Wei Zhu¹
¹ School of Electronic and Communication Engineering, Sun Yat-sen University, Shenzhen 518107, China; zhuxw666@mail.sysu.edu.cn, zhengzh53@mail2.sysu.edu.cn

² School of Aeronautics and Astronautics, Sun Yat-sen University, Shenzhen 518107, China

³ School of Systems Science and Engineering, Sun Yat-sen University, Guangzhou 510275, China

Received 2023 October 25; revised 2023 November 29; accepted 2023 December 5; published 2024 March 4

Abstract

In today's society, there is a wide demand for high-precision and high-stability time service in the fields of electric power, communication, transportation and finance. At present, the time standard in various countries is mainly based on atomic clocks, but the frequency drift of atomic clocks will affect the long-term stability performance. Compared with atomic clocks, millisecond pulsars have better long-term stability and can complement with the excellent short-term stability of atomic clocks. In order to improve the long-term stability of the atomic timescale, and then improve the timing accuracy, this paper proposes an algorithm for steering the atomic clock ensemble (ACE) by ensemble pulsar time (EPT) based on digital phase locked loop (DPLL). First, the ACE and EPT are generated by the ALGOS algorithm, then the ACE is steered by EPT based on DPLL to calibrate the long-term frequency drift of the atomic clock, so that the generated steered atomic time follows both the short-term stability characteristics of ACE and the long-term stability characteristics of EPT, and finally, the steered atomic time is used to calibrate the local cesium clock. The experimental results show that the long-term stability of atomic time after steering is improved by 2 orders of magnitude compared with that before steering, and the daily drift of a local cesium clock after calibration is less than 9.47 ns in 3 yr, 3 orders of magnitude higher than that before calibration on accuracy.

Key words: (stars:) pulsars: general – time – methods: data analysis – instabilities

1. Introduction

High-precision timing is realized on the basis of establishing a high-accuracy and high-stability timescale, which is widely used in power, communication, transportation, finance and other fields. High-precision time reference is mainly generated by the joint use of atomic clocks, including common atomic clocks such as a rubidium clock, hydrogen clock or cesium clock, which have good short-term stability and small timing error in a short time of self-timekeeping. However, due to the long-term frequency drift of atomic clocks, in the scenario of long-term self-timekeeping, atomic clocks and timekeeping systems based on atomic clocks will produce more and more serious frequency drift and phase deviation, resulting in increasingly large 1 pulse per second (1PPS) timing errors. Coordinated Universal Time (UTC) is a widely used atomic time (AT), and the local timekeeping laboratory regularly sends the atomic clock comparison data of UTC 0h every day to the Bureau International des Poids et Mesures (BIPM). BIPM obtains the time difference between the local AT data and the international comparison center station through the remote time comparison link, and obtains the weighted average free AT. International Atomic Time (TAI) is calibrated with a fountain clock, and UTC is obtained by a leap second (Zhang et al. 2020).

Pulsars are high-speed rotating neutron stars with excellent long-term rotational stability. Pulsar signals are used to steer atomic clocks and generate timescales that take both long-term and short-term stability into account. The high-precision real-time observation of pulsar times of arrival (TOAs) by advanced telescopes such as FAST can avoid the lag problem of precise timekeeping sources such as UTC and Terrestrial Time at BIPM (TT(BIPM)), and can be further applied as timing signal sources in deep space navigation, power grid, intelligent transportation and other fields to achieve high long-term stability and high-precision timing (Luo et al. 2021; Qiu et al. 2022; Yang et al. 2022). In addition, pulsar pulse signals are much more complex than global navigation satellite system (GNSS) timing systems that can be easily identified by machine learning methods (Tariq et al. 2022), and pulsars can serve as auxiliary signal sources if the existing atomic clock timing system is deliberately destroyed or tricked, or loses its lock in areas with weak signals (Qiu et al. 2022). The generation of pulsar time (PT) is based on the pulsar timing observation data and ephemeris data, and the difference between the predicted pulse TOA and the observed value at the solar system's centroid is obtained, that is, the timing residual. Here, the predicted value is the PT generated by the pulse phase model, and the observed value is based on local AT, so if all error terms are corrected, the timing residual is equal to the

difference between PT and AT (Zhou et al. 2021a, 2021b). By tracing the AT recorded by the atomic clock of the station to TAI, the clock error between PT and TAI is obtained. By combining the timing residuals of multiple pulsars with some algorithm, the ensemble pulsar time (EPT) can be established.

Based on the characteristics of PT and AT, and the complementary characteristics of stability, the combination of PT and an atomic clock can improve the accuracy and stability of time reference. In recent years, in the main research on utilizing pulsars and atomic clocks for joint timekeeping or timing, Liu et al. (2023) proposed using Vondrak–Cepek filtering to combine PT and AT to generate a timescale with good short-term stability and long-term stability, but the timescale generated by the algorithm lags behind and the real-time performance is insufficient. Li et al. (2023) relied on the dual-steering algorithm to steer an atomic clock by pulsars, in which the monthly steer is closed-loop, which ensures the real-time performance of the time reference after steering (Dong 2020). However, the pulsar timing residual in this paper is a simulation of future data, and the longer the prediction time, the less credible the sequence is.

In this paper, an algorithm based on the digital phase locked loop (DPLL) for steering the AT is proposed. The atomic clock signal is set as the local oscillator of DPLL, and the pulsar signal is set as the steering frequency source of DPLL. Most of the low-frequency noise of the atomic clock and most of the high-frequency noise of the pulsar are filtered by the loop filter, and a timescale combining the advantages of the two is generated, so as to generate a high-precision timing signal and provide 1PPS for timing sources such as power grid terminals.

The parts of this paper are arranged as follows: Section 2 introduces the principle of timekeeping algorithms, including the EPT algorithm and atomic clock ensemble (ACE) algorithm. Section 3 introduces the principle of pulsar steering algorithm based on DPLL. In Section 4, an experiment is carried out and the results are analyzed. The clock errors of EPT(1PPS), ACE(1PPS) and (ACE+EPT)(1PPS) based on DPLL are calculated, and a local cesium clock is calibrated with (ACE+EPT)(1PPS) to achieve high-precision daily drift, and the error between the experiment and the actual timing situation is analyzed. Section 5 summarizes this article.

2. Principle of Timekeeping Algorithm

This section introduces the basic principles of a timekeeping algorithm, including the EPT algorithm and ACE algorithm. Among those, the ALGOS algorithm is the basis of clock error weighting for pulsars and atomic clocks, and the corresponding 1PPS clock error signals are generated by the EPT algorithm and ACE algorithm respectively, which are used as the external frequency source and local frequency source of DPLL.

The calculations of EPT and ACE need several pulsar clocks and atomic clocks respectively. When using these two clock groups to calculate the average timescale, methods such as ALGOS, Kalman filtering, and wavelet analysis can be applied. The ALGOS algorithm, as a typical weighted average algorithm, can improve the stability of EPT and ACE, so it is employed to calculate the comprehensive timescale. In this algorithm, the Allan variance used to calculate atomic clocks and the statistical method of $\sigma_z(\tau)$ variance (also known as Hadamard variance) used to calculate pulsar clocks are expressed as Equations (1) and (2) respectively (Allan 1966; Demetrios et al. 1997)

$$\sigma_y^2(\tau) = \frac{1}{2(N-2)\tau^2} \sum_{i=1}^{N-2} [x(i+2) - 2x(i+1) + x(i)]^2, \quad (1)$$

$$\sigma_z(\tau) = \frac{\tau^2}{2\sqrt{5}} \langle c_3^2 \rangle^{1/2}. \quad (2)$$

Among them, the residual and error are divided into subsequences with equal intervals of τ , and each subsequence is fitted by a cubic polynomial, where c_3 is the coefficient of the highest term, and $\langle \rangle$ is expressed in all subsequences, and the average value is taken as the weight inversely proportional to the square of c_3 error.

Pulsars have sizable, a priori unknown frequency drifts, so Allan variance is not particularly suitable for pulsar data (Demetrios et al. 1997). By defining one more difference from the Allan variance, $\sigma_z(\tau)$ variance ignores the fixed frequency drift in the pulsar timing residuals.

2.1. Ensemble Pulsar Time Algorithm Flow

In this section, first, the timing residual of the selected pulsar is used to generate EPT, which is traced back to TAI through TT(BIPM19) and converted to UTC, and then interpolated into EPT(1PPS) clock error signal as the steering frequency source of DPLL. The detailed flow chart is shown in Figure 1.

In order to improve the accuracy of the final EPT(1PPS) timekeeping, according to the indexes of “more observation points” and “longer observation time” proposed by Shaifullah et al. (2022), M better pulsars are selected as frequency sources. Due to the strict linear relationship between PT and timing residual, we can use the Tempo2 software (Edwards et al. 2006; Hobbs et al. 2006, 2009) to fit the observation data and calculate the timing residual traced back to TT(BIPM19).

Due to the large timing noise of a single pulsar, the timing stability can be improved by weighting. Therefore, it is necessary to set the reference pulsar to Modified Julian Date (MJD), and align the timing residuals and errors of other pulsars to the MJD reference by down-sampling. In order to calculate the clock error of EPT(1PPS) with EPT, it is

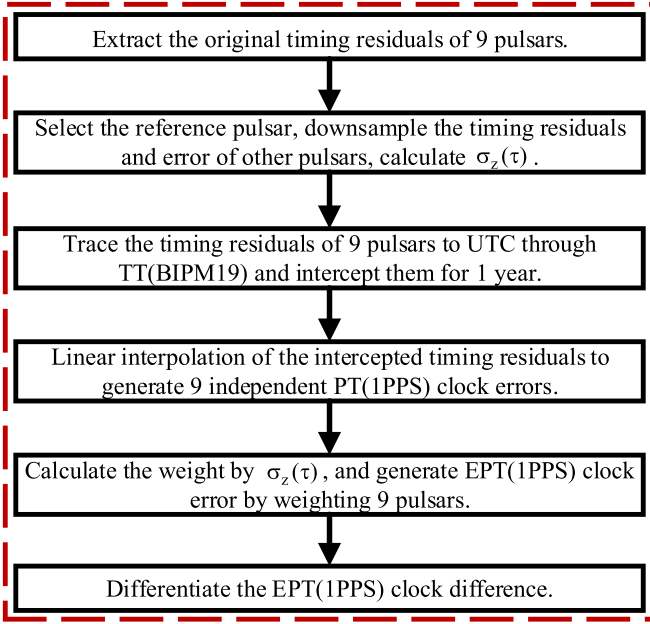


Figure 1. Calculation flow chart of EPT(1PPS).

necessary to linearly interpolate the timing residuals and errors with the interval of 1PPS by MJD, so that the interpolation of subsequent timing residuals can meet the condition of equal interval and reduce the errors.

Because the purpose of this paper is timing, it is necessary to align the past 1PPS signals of EPT and ACE and input them into the DPLL steering algorithm to fix their time series length. When adding the latest value, the earliest value is discarded. In order to calculate the long-term stability, the $\sigma_z(\tau)$ method should be used to evaluate the stability before truncation for weighting, so as to eliminate the frequency drift of the pulsar.

Since the AT has been traced back to UTC, and the pulsar signal is traced back to TT(BIPM19), it is only necessary to trace the PT back to UTC, so that the time reference of the steering operation can be unified. The interval of traceability data between TT(BIPM19) and UTC provided by BIPM is 10 days (Rodin 2008), with larger intervals, so it is necessary to linearly interpolate the timing residual points to calibrate the deviation from UTC. Then, we intercept the data according to the preset time series length.

To facilitate interpolation, create an MJD index table such that the horizontal axis is a 1PPS time series, the minimum value of the vertical axis is 0 and the maximum value is the number N of timing residuals within the set MJD range. Distribute the abscissa of the 1PPS signal (1, 2, ...) evenly to the gaps in timing residuals.

Let the abscissa of an interpolation point be x and the interpolation be y . If the abscissa of the original residual is replaced by x_1, x_2, \dots, x_N and the ordinate corresponds to $y_1,$

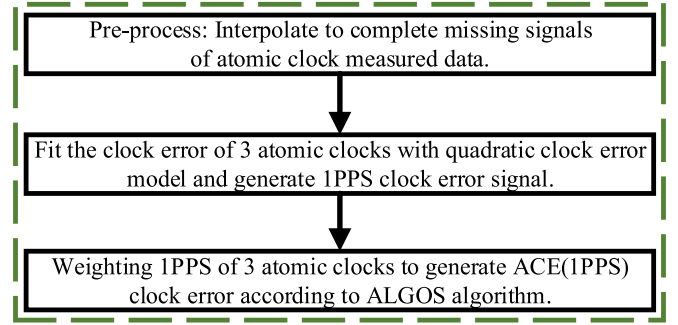


Figure 2. Calculation flow chart of ACE(1PPS).

y_2, \dots, y_N respectively, the interpolation formula can be obtained

$$y = \begin{cases} y_1 - \frac{x_1 - x}{x_2 - x_1}(y_2 - y_1), & x < x_1 \\ y_k + \frac{x - x_k}{x_{k+1} - x_k}(y_{k+1} - y_k), & x_1 \leq x \leq x_N \\ y_N + \frac{x - x_N}{x_N - x_{N-1}}(y_N - y_{N-1}), & x > x_N \end{cases} \quad (3)$$

After the PT (1PPS) clock error of each pulsar is obtained by interpolation, the normalized weights w_i are calculated based on the ALGOS algorithm, so that the clock error of M pulsars can be weighted to calculate the EPT(1PPS) clock error, and weaken the instability brought by a single pulsar (Petit et al. 1993; Panfilo & Arias 2019).

Finally, the EPT(1PPS) clock error needs to be differentiated to obtain the frequency difference, so as to complete the steering of the ACE(1PPS) phase in the subsequent DPLL steering algorithm. Because the pulsar signal is used as the steering frequency source, the steering physical quantity that needs to be provided is the frequency, not the phase. Since the EPT(1PPS) resulting from this step is a differential frequency signal, $\sigma_z(\tau)$ is no longer required for subsequent evaluation of its stability, but only Allan deviation. While the generated (ACE+EPT)(1PPS) has an even smaller frequency drift, Allan deviation can also be used to calculate stability.

After the above steps, the real-time availability of the EPT signal is realized, and at the same time most of the original timing residuals of each pulsar are preserved, which are used as the steering frequency source of the subsequent DPLL algorithm.

2.2. Atomic Clock Ensemble Algorithm Flow

In this section, first, the measured clock error of the pretreated atomic clock is fitted and interpolated by a quadratic model, and the noise is added at the interpolation point and weighted based on Allan deviation, which is used as the local oscillation signal of DPLL. The detailed flow chart is shown in Figure 2.

First, the actual clock errors of atomic clocks should be analyzed in detail, the clock error data with obvious abnormal values should be eliminated and linear interpolation should be performed for very few clock error missing points. If the

original data are normal, skip this step. This step can ensure the normal progress of subsequent data processing, and at the same time, due to the small number of abnormal data points, the impact on the original data can be ignored.

If the time interval of the original data is too long, it needs to be interpolated into 1PPS clock error. Generally, atomic clocks have clock drift that deteriorates with time, so the quadratic clock error model (Galleani et al. 2003) is often used to model them, and the approximation of clock error, clock speed and clock drift parameters is completed. The expression is as follows

$$x(t) = x_0 + y_0 t + \frac{1}{2} dt^2 + \varepsilon_x(t). \quad (4)$$

Here x_0 , y_0 and d are initial time error, frequency error and linear frequency drift, respectively, which are deterministic components, and the rest are noise.

In order to steer the atomic clock by pulsars, it is necessary to align the MJD of the selected atomic clock with the MJD of EPT(1PPS) clock error by interception, and interpolate the clock error of the atomic clock into 1PPS clock error with the fitted parameters. Similar to the data processing method of a pulsar, Allan deviation (Allan 1966) can be calculated according to historical observation data before intercepting the atomic clock error, so as to calculate the more accurate weight of each atomic clock. If the 1PPS signal can be obtained directly in the original observation, this step can be skipped.

Based on the ALGOS algorithm, the weight of each clock can be obtained by Allan deviation after generating the AT(1PPS) clock error, and then the ACE(1PPS) clock error can be generated by weighting. After the above steps, the 1PPS matching between the ACE signal and the EPT signal is realized, and it is used as the local oscillator frequency source of the subsequent DPLL algorithm.

3. Principle of Pulsar-steering Algorithm Based on DPLL

This section introduces the algorithm principle from time-keeping to timing. The timekeeping algorithm completes the steer of EPT(1PPS) to ACE(1PPS) based on DPLL, in which the steering frequency source and local oscillator frequency source of DPLL are static. The timing algorithm is based on (ACE+EPT)(1PPS) of steering output, which periodically calibrates the clock error of a local cesium clock and realizes the dynamic output of actual physical signals.

3.1. Principle of Loop Establishment and Steering of DPLL

DPLL is a negative feedback system, which can steer the phase of a local oscillator through the phase of the input signal source. Its basic structure is illustrated in Figure 3 (Prasad & Sharma 2012).

Among that, PD, LPF and VCO are phase detectors, loop filters and voltage-controlled oscillators, respectively. The

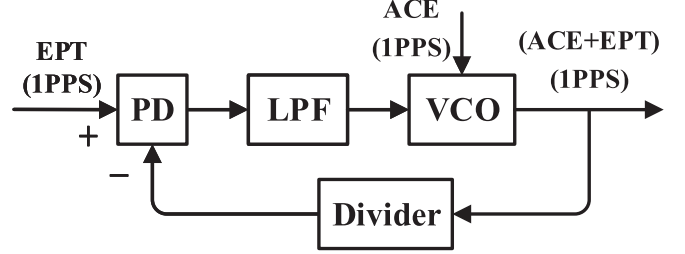


Figure 3. DPLL schematic diagram.

product of the gains of the three is recorded as $G(z)$, which represents the transfer function of the DPLL open-loop system in the Z domain; EPT(1PPS) stands for the reference input of DPLL, also known as the steering frequency source; ACE (1PPS) represents the local oscillator frequency source of DPLL, input to the VCO; (ACE+EPT)(1PPS) is the output after steering, fed back to the input terminal through the frequency divider. By analyzing the I/O characteristics of the DPLL system in Z domain, the output of DPLL can be expressed as

$$\begin{aligned} (\text{ACE} + \text{EPT})(z) &= \frac{G(z)}{1 + G(z)} \text{EPT}(z) + \frac{1}{1 + G(z)} \text{ACE}(z) \\ &= H(z) \text{EPT}(z) + H_e(z) \text{ACE}(z). \end{aligned} \quad (5)$$

Here $H(z)$ is the transfer function of the closed-loop system, and it is a low-pass filter, which can filter out the high-frequency noise in the clock error of the steering frequency source EPT(1PPS). $H_e(z)$ is the closed-loop error transfer function of DPLL, and it is a high-pass filter, which can filter out the low-frequency noise in the clock error of local oscillator frequency source ACE(1PPS). Therefore, the steered (ACE +EPT)(1PPS) clock error has small low frequency noise and high frequency noise at the same time.

Considering that the third-order phase-locked loop can stably track the frequency ramp-up signal (Lu 2016), and its performance is better than that of the second-order phase-locked loop, which can ensure the steering stability of ACE (1PPS) with EPT(1PPS) clock error in this paper, the system transfer function of DPLL is selected from Feng et al. (2021)

$$\begin{aligned} H(z) &= \frac{K_d K_0}{1 - z^{-1}} \left(\frac{2\tau_2 + T}{2\tau_1} + \frac{T}{\tau_1} \frac{z^{-1}}{1 - z^{-1}} \right) \\ &\quad \times \left(\frac{T}{2\tau_3 - T} \frac{1 + z^{-1}}{1 - z^{-1}} \right). \end{aligned} \quad (6)$$

Here T is the sampling period, K_d is the gain of the phase detector, K_0 is the gain of the voltage steered oscillator and the intersection bandwidth of the system transfer function is

$$K = \frac{K_d K_0 \tau_2}{2\pi \tau_1}. \quad (7)$$

The optimal loop parameters (Shen 2018; Feng et al. 2021) are obtained when and only when the single sideband phase noise intersection of ACE(1PPS) and EPT(1PPS) is equal to K . At this time, (ACE+EPT)(1PPS) simultaneously retains the near-end phase noise of EPT(1PPS) and the far-end phase noise of ACE(1PPS), and the steering effect is the best.

In the actual timing scenario, according to the dynamic change of input sequence, the value of K is automatically adjusted according to the calculation formula of loop parameter, and the loop can remain stable. When the output signal is in the first steering cycle, the 1PPS clock error of the steered source ACE is output. In the following steering cycle, the frequency of ACE(1PPS) is feedback steered by calculating the difference between the frequency of EPT(1PPS) and that of ACE(1PPS), thus avoiding the uncontrollable phase drift of ACE(1PPS). At the same time, using the excellent short-term stability of ACE (1PPS) clock error, a lot of high-frequency noise of EPT(1PPS) clock error is eliminated, and the second-order difference of the output signal is similar to that of ACE(1PPS) clock error.

3.2. Daily Drift Calibration of Local Cesium Clock Error

In the last section, the (ACE+EPT)(1PPS) clock error signal in the past year was obtained by DPLL. However, only the 1PPS clock error in the last second of this output signal can be used for timing, because only the 1PPS clock error in the last second of the two input signals is real-time. Although the clock error of an atomic clock is better predicted according to the model, pulsars are affected by various complex factors, and the uncertainty of clock error prediction is too strong (Demetrios et al. 1997), so it is difficult to accurately generate future 1PPS clock error signals. Therefore, the clock error of (ACE+EPT)(1PPS) in the last second is selected, and then the one with the smallest daily drift among L atomic clocks is selected, and the (ACE+EPT)(1PPS) clock error is used as its calibration source to obtain $Cs_{steered}(1PPS)$.

When the DPLL runs once a day, first, the ACE(1PPS) clock error and EPT(1PPS) clock error of that day should be introduced in the same way, and the clock error of the earliest day should be deleted. Then the initial phase of the current one-year sequence is calibrated to UTC released one year lagged. Finally, the 1PPS clock error in the last second is calculated by the same method. At this time, the local master clock is calibrated by the method of phase microjump (Fang et al. 2022) to avoid the loss of lock and the deterioration of stability caused by phase step. Therefore, the final daily clock error is the sum of the daily phase offset and calibration error of the local atomic clock.

3.3. Algorithm Flow of Pulsar Steering Atomic Clock Based on DPLL

The flow chart of clock error steering algorithm based on DPLL is depicted in Figure 4.

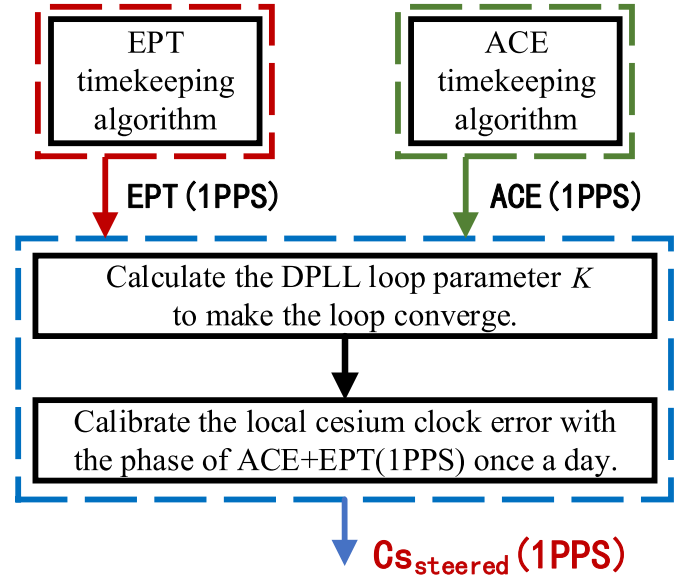


Figure 4. Flow chart of ACE(1PPS) calculation.

These include EPT algorithm, ACE algorithm and clock error steering algorithm based on DPLL. The final generated $Cs_{steered}(1PPS)$ is the output signal of this algorithm, which is used for high-precision timing. The clock error steering algorithm based on DPLL is as follows.

Step 1. Calculation of ACE(1PPS) and EPT(1PPS);

Step 2. Based on the steering of DPLL clock error, the timekeeping signal of (ACE+EPT)(1PPS) is generated;

Step 3. Calibrate the local cesium clock periodically with (ACE+EPT)(1PPS) to complete high-precision time service.

To sum up, the algorithm in this paper can be summarized as: EPT timekeeping algorithm represented by red dotted line box, ACE timekeeping algorithm represented by green dotted line box and DPLL-based clock error control algorithm represented by blue dotted line box. Although the algorithm is relatively complicated, it can realize automatic processing in the actual time service process, which can generate real-time time service scale with better accuracy and long-term stability than atomic clocks.

4. Experiments and Results Analysis

This section first introduces the source and selection of the data used, and then gives the calculation and analysis of EPT (1PPS) frequency error and ACE(1PPS) clock error respectively. Finally, the EPT(1PPS) frequency error is used to steer the ACE(1PPS) clock error through DPLL, and the local cesium clock is calibrated daily with the generated signal, and the robustness of loop parameter is analyzed. In each data processing link, the error compared with the actual timing system is analyzed.

Table 1
Key Parameters of Nine Pulsars (Arzoumanian et al. 2015)

PSR Name	Span/yr	TOAs	MJD Range (days)
J0437-4715	13.50	5302	51770–56705
J0613-0200	16.05	9322	50932–56796
J1012+5307	16.83	13056	50647–56795
J1643-1224	20.14	8136	49422–56778
J1713+0747	22.46	17486	48850–57052
J1744-1134	19.88	9834	49729–56991
J1909-3744	10.82	11483	53041–56992
J1918-0642	12.80	9941	52095–56769
J2145-0750	19.83	8455	49518–56761

4.1. Experimental Data

Pulsar timing data are selected from the pulsar data set (Perera et al. 2019; Antoniadis et al. 2022) published by IPTA in 2019. According to Shaifullah et al. (2022), J0437-4715, J0613-0200, J1012+5307, J1643-1224, J1713+0747, J1744-1134, J1909-3744, J1918-0642 and J2145-0750 are selected from 65 pulsars. The key parameters of the selected pulsar are shown in Table 1.

Among them, the observation range and TOA data points of the above pulsars are better in the pulsar data set, and the MJD range can cover the selected atomic clock data.

AT data were obtained from the BIPM official website (<https://webtai.bipm.org/ftp/pub/tai/data/>), and three atomic clocks (Cs1350104, Cs1351463 and H1400711) from the United States Naval Observatory were selected (Liu et al. 2023). The MJD range was 53739–55584, and the sampling period of clock error was 5 days. Among them, the data of cesium clock Cs1350104 are normal, while the other two clocks are missing less than 3% of the data. It is necessary to linearly interpolate these data, and then add noise with the average value of the second difference of the clock error as the average value, and then calculate the Allan deviation of each atomic clock error. The key parameters of the selected atomic clock are shown in Table 2.

Because the DPLL steering algorithm requires two input frequency sources to have the same start and end time and the same data length, it is necessary to intercept the pulsar and atomic clock data with the same MJD respectively when verifying the feasibility of the algorithm. The ranges of three groups of MJD used in this paper are 53739–54104, 54104–54469 and 54469–54834, respectively, and the length is one year.

4.2. Experiment and Result Analysis

4.2.1. Performance Analysis of EPT(1PPS) Clock Error

This section analyzes the performance of EPT.

Considering that the release time of UTC is one year behind, the timescale of 1PPS clock error is set to one year, so that the initial phase of DPLL local oscillator is aligned with the latest

Table 2
Key Parameters of Three Atomic Clocks

Atomic Clock Name	Sampling Points	Sampling Period (days)	MJD Range (days)	Data Missing Ratio
Cs1350104	360	5	53739–55534	0%
Cs1351463	360	5	53739–55584	2.78%
H1400711	360	5	50647–55564	1.67%

UTC. Since the AT data start from MJD 53739, in order to ensure a real-time and causal system, the residual of each pulsar after MJD 54104 is removed. J1909-3744 with the least number of residual points is selected as the benchmark of MJD to ensure the authenticity of timing residuals. Align the MJD of the other eight pulsars to the benchmark, then downsample and linearly interpolate the timing residuals and errors, then calculate the $\sigma_z(\tau)$ variance of each pulsar. To maximize the use of the properties of the pulsar's long-term stability, the EPT is weighted by the inverse of the end value of $\sigma_z(\tau)$. The $\sigma_z(\tau)$ variance of nine pulsars and EPT are displayed in Figure 5(a).

From the curve of EPT, it can be seen that the short-term stability and long-term stability of EPT are close to the pulsar with the best performance, especially on the one-year scale, and its $\sigma_z(\tau)$ stability is better than all pulsars. Therefore, weighting the timing residual can smooth the uncorrelated timing noise of multiple pulsars and make EPT more stable than what is allowed by a single pulsar. At the same time, setting the length of pulsar timing residual to one year can ensure smaller timing error and better stability.

IPTA Data Release 2 (DR2), the pulsar data set selected in this paper, has been traced back to TT(BIPM19). The calibration deviation of tracing is expressed as $\Delta t(\mu\text{s})$, then we have

$$\begin{cases} \Delta t = \text{TT(BIPM19)} - \text{TAI} - 32.184 \text{ s} \\ \text{UTC} = \text{TAI} - 37 \text{ s} \end{cases}, \quad (8)$$

so that the PT can be traced back to UTC. Subsequently, the traced timing residual between MJD 53739 and MJD 54104 is intercepted.

Based on MJD benchmark pulsar J1909-3744, the number of points for the timing residual is 1060. We substitute $N = 1060$ into Equation (3), interpolate the timing residual to generate PT(1PPS) clock error and then add the evenly distributed random noise. We then substitute $M = 9$ into the ALGOS algorithm to calculate the EPT(1PPS) clock error and calculate the frequency error through difference. The clock error of EPT (1PPS) is shown in Figure 5(b). From this figure, we can see that compared with the clock drift phenomenon of atomic clocks, the clock drift of pulsars is not obvious, and the UTC traceability error on a one-year scale is still in the microsecond

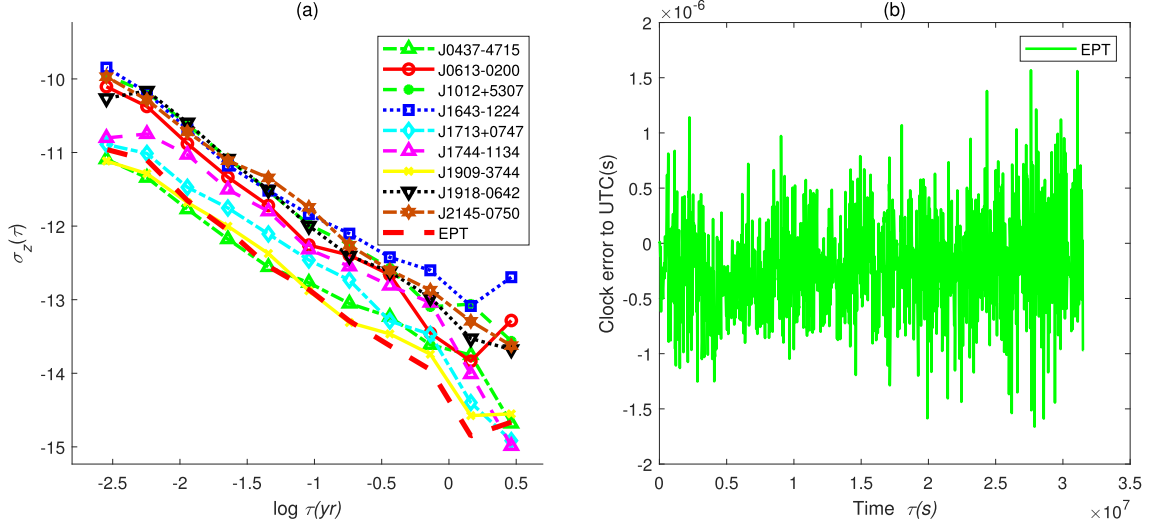


Figure 5. $\sigma_z(\tau)$ variance and EPT clock error of pulsars before and after weighting. (a) $\sigma_z(\tau)$ variance of nine pulsars and EPT. (b) EPT clock error.

order, indicating that the long-term clock drift of atomic clocks can be calibrated by pulsar signals.

To sum up, the stability and clock error of EPT(1PPS) are better than those of a single pulsar.

When actually calculating the EPT(1PPS) clock error, there are differences in data processing methods or systematic errors in the following steps:

- (1) When extracting the timing residuals of pulsars, it is necessary to use an astronomical telescope to collect the TOA and ephemeris data in real time, and generate the .tim file and .par file to calculate the timing residual (Edwards et al. 2006). Because the pulsar observation accuracy of the FAST facility has surpassed the data source IPTA (Yang et al. 2023) in this paper, the accuracy of timing residuals can be improved by establishing cooperation with similar observation stations.
- (2) When the reference star is selected by MJD and the other stars are down-sampled, the signal acquisition interval of the IPTA data set is uneven, the frequency band coverage is incomplete and the observation accuracy is limited (Perera et al. 2019), but in reality, the telescope continuously collects signals in real time, so the influence of this step on the timing residual will be reduced.
- (3) When tracing the residual to UTC through TT(BIPM19) and truncation, due to the inability to obtain TT(BIPM23) in real time, it can only be based on the calculation formula in TT(BIPM21)

$$\text{TT(BIPM21)} = \text{TAI} + 32.184 \text{ s} + 27667.5 \text{ ns} - 0.01(\text{MJD} - 59579)\text{ns}, \quad (9)$$

to trace TT to TAI and further trace it to UTC. Since the difference between the predicted value and the actual value of TT (BIPM21) is between -6.2 ns and -0.2 ns ,

Table 3
Deterministic Parameter Fitting of Three Atomic Clocks

Atomic Clock Name	x_0	y_0	d
Cs1350104	4.1146×10^{-5}	6.7652×10^{-8}	6.2721×10^{-11}
Cs1351463	1.7747×10^{-5}	4.4457×10^{-8}	3.7925×10^{-11}
H1400711	3.7494×10^{-4}	9.9961×10^{-7}	7.6749×10^{-10}

the error will increase slightly in the actual timing system, but it is stable and controllable.

- (4) When linearly interpolating the residual and generating the PT(1PPS) clock error, the traceability error is less than 1%, corresponding to the original timing residual, so the interpolation effect brought by the sampling uniformity of the timing residual will be more significant.
- (5) When generating the EPT(1PPS) clock error based on the residual stability weighting, the calculation error of the $\sigma_z(\tau)$ weight will be reduced because the TOA interval of the real-time observation of the pulsar array is more uniform, which makes the calculation more accurate.

Generally speaking, the clock error calculation of EPT (1PPS) can be more accurate through the above steps.

4.2.2. Performance Analysis of ACE(1PPS) Clock Error

This section analyzes the performance of ACE.

According to the quadratic clock error model of Equation (4), the clock errors are fitted, and the results are shown in Table 3, with complete clock interpolation based on the fitting parameters.

Because this paper mainly uses the short-term stability of atomic clocks, the starting point of Allan deviation of each clock is substituted into the ALGOS algorithm, and the normalized weights of Cs1350104, Cs1351463, and H1400711

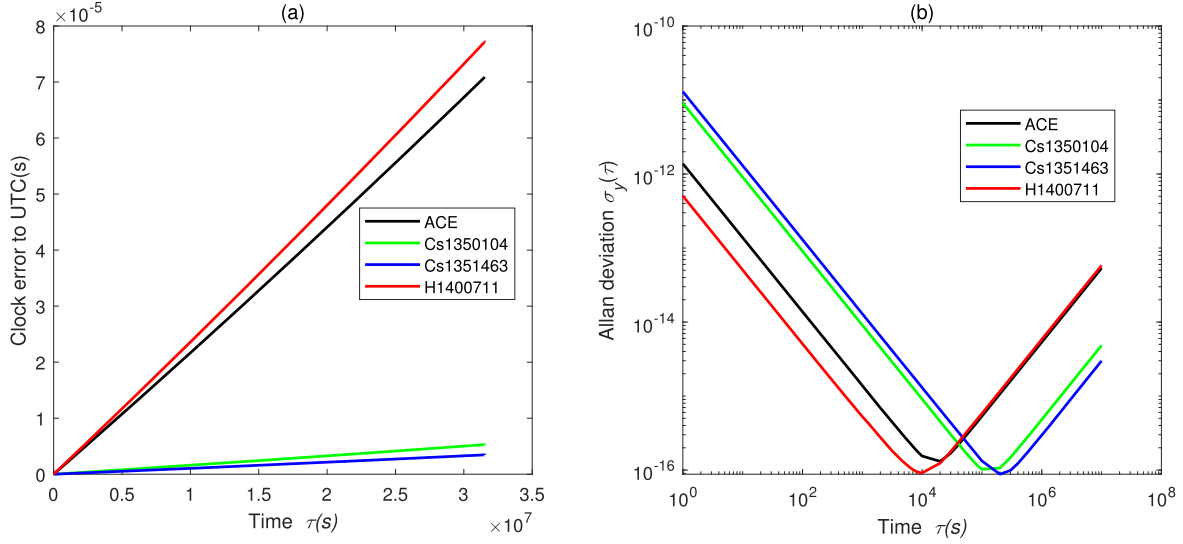


Figure 6. Clock errors between three atomic clocks and ACE(1PPS) and their Allan deviations. (a) Clock errors. (b) Allan deviations.

are obtained as follows: 0.0509, 0.0356 and 0.9135 respectively. After generating the ACE(1PPS) clock error by weighting, we can plot it together with the clock errors of three atomic clocks as shown in Figure 6(a), and display the ACE(1PPS) clock error and the Allan deviation of three atomic clocks together as featured in Figure 6(b).

In Figure 6(a), due to the high weight of H1400711, the clock error of ACE(1PPS) is close to it, and the relative UTC deviation of ACE is smaller than that of a cesium clock in the short term and hydrogen clock in the long term. The secondary clock error model is still dominant in the ACE, but the random noise term contained in it determines the magnitude of the Allan deviation diagram curve shown in Figure 6(b), and it can be concluded that the short-term stability of the ACE is better than that of the cesium clock. Moreover, the long-term stability is better than that of a hydrogen clock, and it is better than that of a single atomic clock as a whole.

When actually calculating the ACE(1PPS) clock error, there are differences in data processing methods or systematic errors in the following steps:

- (1) In the selection of the measured clock error of atomic clocks, data from the National Time Service Center (NTSC) can be used instead (Zhang et al. 2020), and the time service stability and system robustness can be improved by increasing the number of atomic clocks. At the same time, NTSC has more public timing data, and even if the 1PPS signal cannot be read directly, the 1PPS clock error of each clock can be approximately solved by matrix operation. Therefore, the error in the actual timing system will be reduced and the system will be more robust.

Table 4
Power Law Spectrum Fitting Results of ACE(1PPS) and EPT(1PPS)

Frequency Source	h_2	h_0	h_{-1}	h_{-2}	h_{-4}
ACE(1PPS)	5×10^{-23}	0	0	5×10^{-38}	3×10^{-50}
EPT(1PPS)	1×10^{-16}	3×10^{-33}	0	0	0

- (2) When the quadratic model is used to fit the clock error and interpolation, if the 1PPS signal can be read directly, this step can be skipped, thus avoiding the simulation error in the statistical sense. Otherwise, the algorithm steps and errors are unchanged.

Generally speaking, the calculation of clock error of ACE (1PPS) in practical engineering will be more accurate than the results in this paper.

4.2.3. DPLL Steering Performance Analysis

This section analyzes the performance of DPLL-based PT steering AT. First, the Allan deviations of ACE(1PPS) and EPT (1PPS) are fitted separately based on the power-law spectrum parameters. The fitting parameters are shown in Table 4, and the fitting curves are displayed in Figure 7(a) and (b). Second, the single sideband phase noise of these two frequency sources is calculated based on the power law spectrum parameters, as shown in Figure 7(c). We calculate the intersection of phase noise to obtain loop parameter K . Finally, based on this parameter, the clock errors of ACE(1PPS), EPT(1PPS), and (ACE+EPT)(1PPS) before and after DPLL steering algorithm are drawn in Figure 7(d), where the EPT(1PPS) clock error represented by the green line is the pulsar clock error curve in

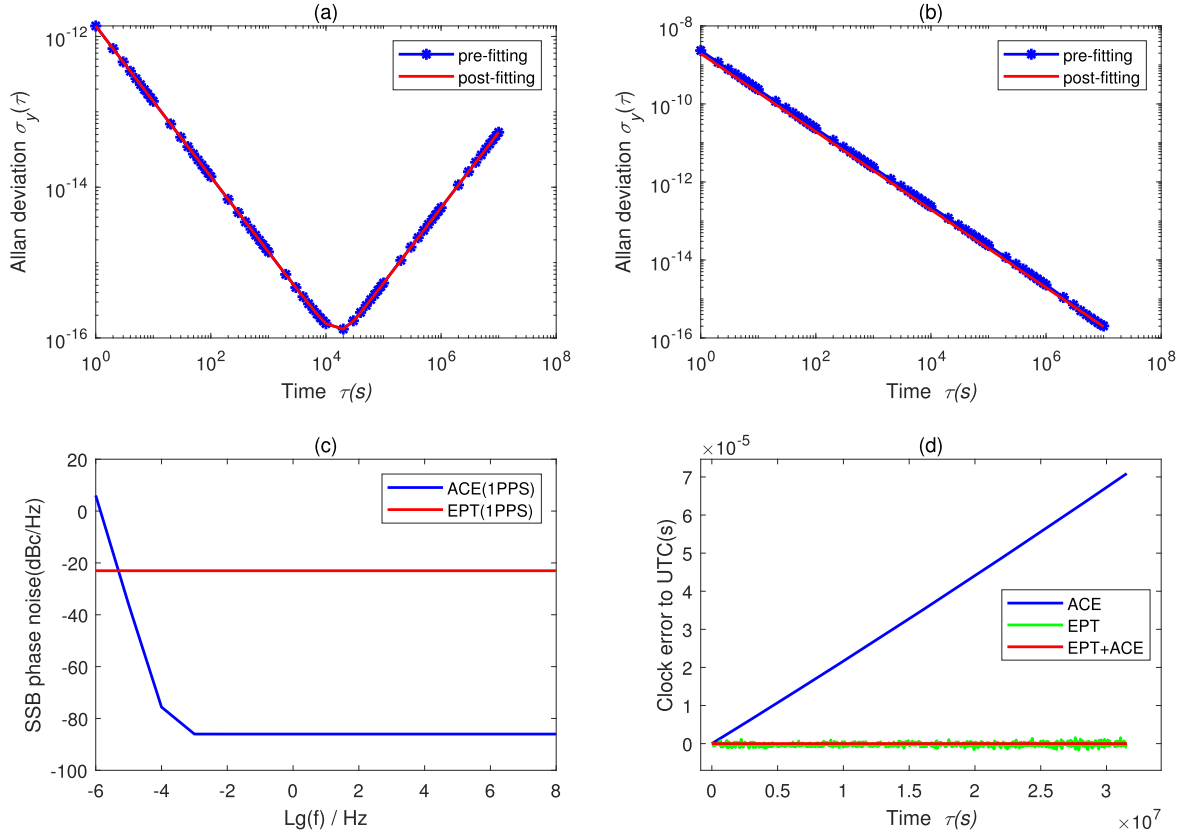


Figure 7. Loop parameter fitting and clock error before and after steering. (a) Allan deviation fitting result of ACE(1PPS). (b) Allan deviation fitting result of EPT(1PPS). (c) Single sideband (SSB) phase noise of ACE and EPT. (d) Clock errors before and after EPT steering ACE.

Figure 5(b). The short-term stability of the blue line and red line is good, and their second-order difference is further compared and verified in Figure 8(a)–(c).

From the fitting results of power law spectrum parameters shown in Table 4, it can be known that there is a small amount of frequency random running noise (h_{-4}) in the ACE(1PPS) clock error, which will greatly reduce the long-term stability of the atomic clock. However, EPT(1PPS) clock error only has phase white noise (h_2) and frequency white noise (h_0), so its long-term stability is much better than ACE(1PPS).

Since Figure 7(a) and (b) complete the accurate fitting of the frequency source, the single sideband phase noise calculated by the power-law spectrum parameters of ACE(1PPS) and EPT(1PPS) is accurate. By taking the intersection of the two curves in Figure 7(c), we can get

$$K = 4.9091 \times 10^{-6}. \quad (10)$$

It can be seen from Figure 7(d) that the (ACE+EPT)(1PPS) clock error shown in the red line overcomes the clock drift defect of ACE, reduces the short-term clock error fluctuation of EPT and realizes the steering of ACE(1PPS) by EPT(1PPS).

In Figure 8, Figure 8(a), representing the second-order difference of ACE(1PPS) clock error, is close to Figure 8(b) representing the second-order difference of (ACE+EPT)

(1PPS) clock error, which demonstrates that the DPLL algorithm keeps the high-frequency part of the former well. Figure 8(d) is obtained by the difference between them. The clock error is reduced by about 2 orders of magnitude, and the curve trend is similar to the second-order difference of the frequency difference of EPT(1PPS), which shows that the algorithm keeps the low-frequency part of the clock error of EPT(1PPS) at the same time.

We can enlarge Figure 8(b) as shown in Figure 9(a), then calculate the Allan deviation of ACE(1PPS) clock error, EPT(1PPS) frequency difference and (ACE+EPT)(1PPS) clock error, as depicted in Figure 9(b).

In Figure 9(a), the clock error of (ACE+EPT)(1PPS) in one year is less than 3.60 ns. In Figure 9(b), the Allan deviation of (ACE+EPT)(1PPS) clock error first follows ACE(1PPS), then is biased by EPT(1PPS) and always follows its slope, and the stability after steering for one day is better than that of two signal sources. As the steering time continues to grow, (ACE+EPT)(1PPS) becomes more and more stable, and the one-year stability is 2 orders of magnitude better than that of ACE(1PPS) before steering.

Although Equation (3) makes it difficult for the interpolated data of EPT to maintain the short-term stability of the original residual, resulting in the short-term Allan variance of EPT to

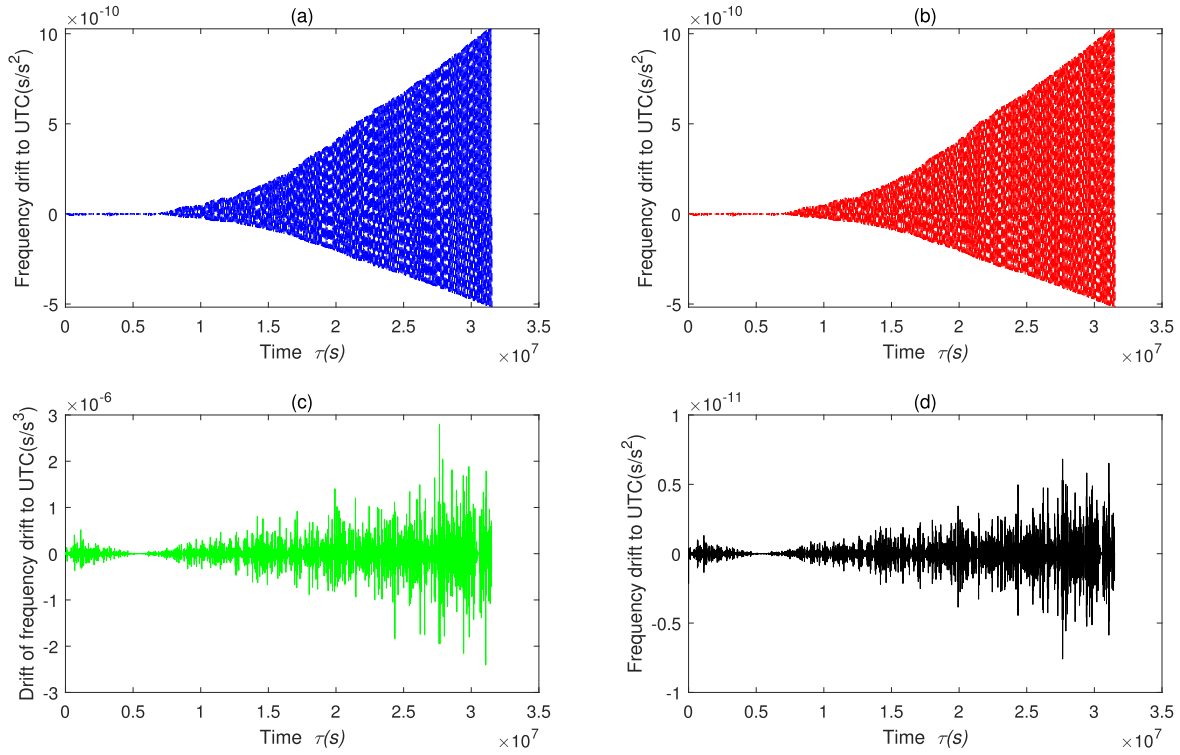


Figure 8. Second-order difference comparison before and after DPLL steering. (a) Second-order difference of ACE(1PPS) clock error. (b) Second-order difference of (ACE+EPT)(1PPS) clock error. (c) Second-order difference of EPT(1PPS) frequency difference. (d) (ACE+EPT)(1PPS) clock error minus the second-order difference of ACE.

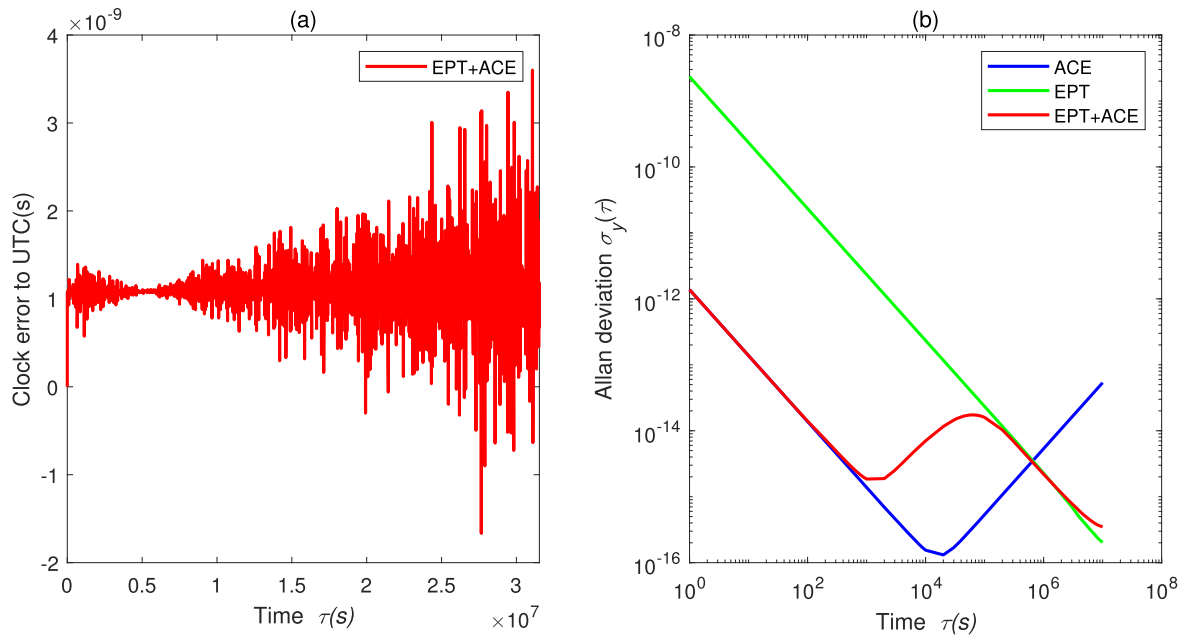


Figure 9. Clock error and Allan deviation of MJD 53739–54104. (a) Clock error after EPT steering ACE. (b) Allan deviation before and after EPT steering ACE.

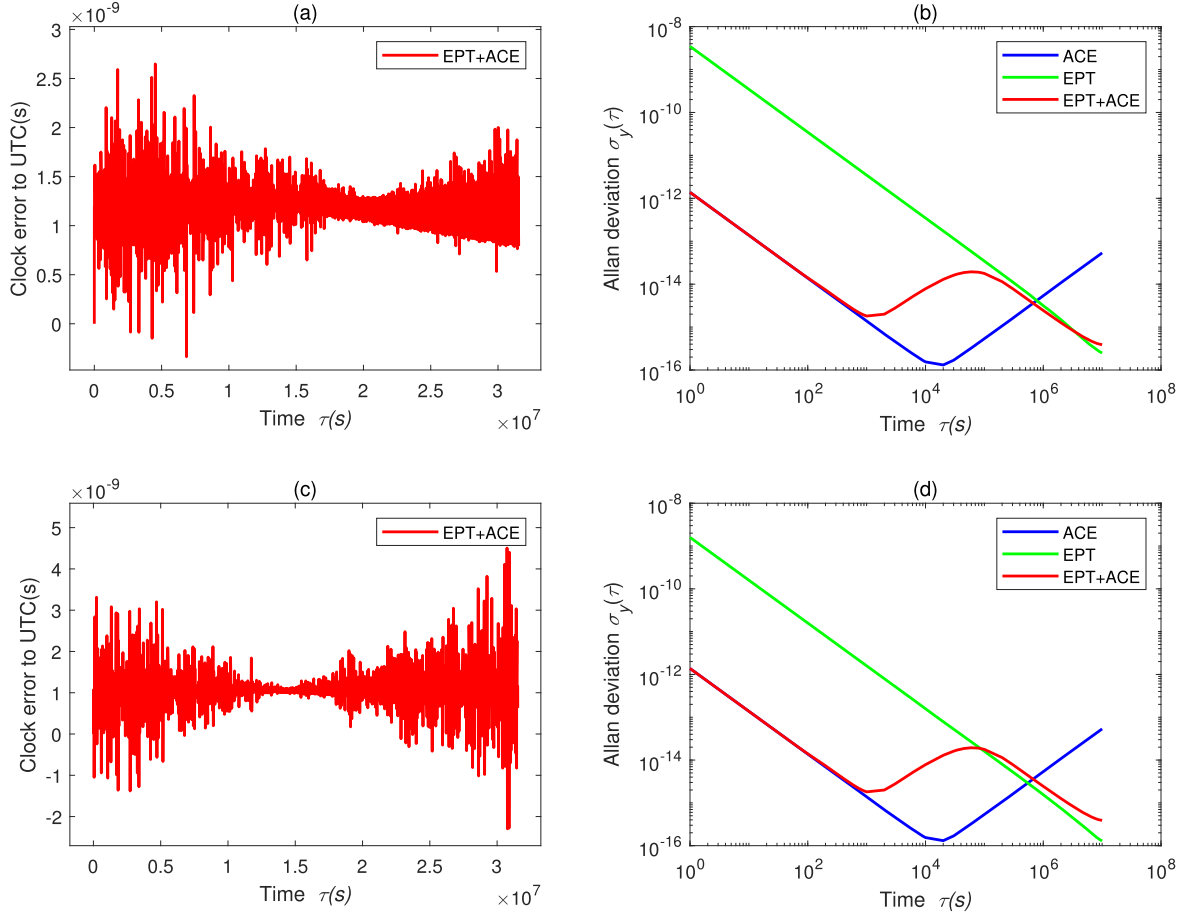


Figure 10. Clock error and Allan deviation in different years. (a) The steered clock error of MJD 54104–54469. (b) The steered Allan deviation of MJD 54104–54469. (c) The steered clock error of MJD 54469–54834. (d) The steered Allan deviation of MJD 54469–54834.

reflect the true value, the Allan variance of (ACE+EPT)(1PPS) follows ACE(1PPS) on a short-term scale and the clock difference of ACE(1PPS) over the steering period. The effect of imprecise and poor Allan variance of EPT can be ignored.

4.2.4. Performance Analysis of Local Cesium Clock Calibration

In this section, based on the (ACE+EPT)(1PPS) of the DPLL steering output, the performance analysis of the clock calibration of the local atomic clock is carried out, so that the steering output has a physical clock carrier and can be applied to the actual timing system. Since the total error of the timing system built in this paper is equal to the steering error plus the error caused by the local atomic clock self-timekeeping, by selecting an atomic clock with the smallest daily drift and performing a DPLL steering operation every single day, the 1PPS timing signal with the best performance can be generated. For the steering error of 3.60 ns in Figure 9(a) (this value is the maximum value on the vertical axis), the cesium clock Cs1351463 with the slowest clock accumulation among the

three atomic clocks (it produces a maximum clock error of 4.73 ns in one day) is selected, and the clock error and the control error are added together, we can see that the daily offset of $Cs_{steered}(1PPS)$ is less than 8.33ns in one year.

Two additional independent experiments were performed below for added confidence. Considering that the timing residual of pulsars is the biggest variable in the steering experiment, the MJD of nine pulsars was directly replaced by 54104–54469 and 54469–54834 in repeated experiments, and the loop parameters were unchanged. We summarize all the variables involved in atomic clocks and pulsars in different years into Table 5, and redraw the clock error and Allan deviation after EPT steering ACE respectively, as shown in Figure 10.

As can be seen from Table 5, the weight of the atomic clock is slightly different in different 3 yr timespans, because the parameters of the atomic clock model are relatively fixed but the noise is random. The main pulsar and the number of residual points are almost unchanged, which demonstrate the system's robustness brought by MJD homogenization. As can be seen from Figure 10(a) and (c), the maximum error of (ACE +EPT)(1PPS) is 4.74 ns, so the daily drift of $Cs_{steered}(1PPS)$ is

Table 5
Comparison of Variables between Atomic Clock and Pulsar in Different Years

MJD Range(days)	Cs1350104's Weight	Cs1351463's Weight	H1400711's Weight	Main Pulsar	Residual Points
53739–54104	0.0508664660822	0.0356065262575	0.9135270076602	J1909-3744	1060
54104–54469	0.0508664660801	0.0356065262561	0.9135270076639	J1909-3744	1060
54469–54834	0.0508664660810	0.0356065262567	0.9135270076624	J1909-3744	1059

less than 9.47 ns in 3 yr, which is 3 orders of magnitude higher than that of microsecond-level daily drift caused by cesium clock independent timing before calibration. As can be ascertained from Figure 10(b) and (d), the Allan deviation of the output after replacing the input sequence still follows the short-term stability of ACE(1PPS) and the long-term stability of EPT(1PPS) steadily, which affirms that the steering based on DPLL is insensitive to the initial loop parameter and the system is robust.

To sum up, the annual stability of AT based on the DPLL steering algorithm is improved by 2 orders of magnitude, and the daily drift accuracy of a local cesium clock calibrated by this signal is improved by 3 orders of magnitude. In the actual time service system, the clock calibration of the local cesium clock cannot jump, so the clock calibration is quadratic, compensated by clock speed and clock drift, and realizes the calibration completely after a period of time. According to the running time of the algorithm, the clock error can be calibrated by calibrating the clock reading at the previous moment, and also by using the method of phase microjump. In addition, the data length and calibration period can be slowly adjusted with the input data to maintain a high-precision time reference.

5. Conclusion

In order to improve the long-term stability and timing accuracy of AT, this paper proposes a pulsar-time-steering algorithm based on DPLL. Pulsar signal and atomic clock signal are used as the steering frequency source and local oscillator frequency source of DPLL, respectively. The finally generated steered frequency source not only avoids the frequency drift of the atomic clock signal, but also reduces the large frequency jitter of pulsar timing residuals in the short term. The experimental results show that, based on the automatic adjustment of loop parameters, the long-term stability of AT after steering follows the signal of EPT (1PPS), and the daily drift of (ACE+EPT)(1PPS) is less than 4.74 ns in 3 yr, and the timing accuracy is improved by 3 orders of magnitude compared with that without calibration. After (ACE+EPT)(1PPS) is used to calibrate the local cesium clock, the daily drift of the clock is less than 9.47 ns. By applying the algorithm used in this paper to atomic clocks with smaller power-law spectrum noise, or introducing the low-frequency filtering method to generate EPT with higher long-term stability (Pizzocaro et al. 2020), higher timing accuracy can be obtained.

The algorithm in this paper can be applied to power grid timing and other fields that need high precision and high stability. In the next step, we only need to replace the historical data used in this paper with the real-time atomic clock error (updated every five days, for example) and the real-time pulsar timing residual, so that we can complete the real-time calibration of the local atomic clock and improve the timing accuracy.

Acknowledgments

This work was supported by the National Key Research and Development Program of China (grant No. 2021YFA0716500), and the National Natural Science Foundation of China (NSFC, grant Nos. 61973328 and 91938301). The authors gratefully acknowledge the support of all individuals and institutions that have supported this work.

References

- Allan, D. W. 1966, *Proc. IEEE*, 54, 221
- Antoniadis, J., Arzoumanian, Z., Babak, S., et al. 2022, *MNRAS*, 510, 4873
- Arzoumanian, Z., Brazier, A., Burke-Spolaor, S., et al. 2015, *ApJ*, 813, 65
- Demetrios, M., Taylor, J., & Eubanks, T. M. 1997, *A&A*, 326, 924
- Dong, J. 2020, *Acta Metrol. Sin.*, 41, 243
- Edwards, R. T., Hobbs, G. B., & Manchester, R. N. 2006, *MNRAS*, 372, 1549
- Fang, W., Jin, S., Chen, D., et al. 2022, *Acta Metrol. Sin.*, 43, 542
- Feng, F., Gong, H., Zang, W., et al. 2021, *GNSS World of China*, 46, 93
- Galleani, L., Sacerdote, L., Tavella, P., et al. 2003, *Metro*, 40, 257
- Hobbs, G., Jenet, F., Lee, K. J., et al. 2009, *MNRAS*, 394, 1945
- Hobbs, G. B., Edwards, R. T., & Manchester, R. N. 2006, *MNRAS*, 369, 655
- Li, B., Qu, L., & Gao, Y. 2023, *AcAau*, 44, 526
- Liu, Y., Xu, B., Zheng, Z., et al. 2023, *MNRAS*, 521, 2553
- Lu, Y. 2016, *Beidou/GPS Dual-mode Software Receiver Principle and Implementation Technology* (Beijing: Publishing House of Electronics Industry) (in Chinese)
- Luo, X., Yin, H., Qiu, W., et al. 2021, in *IEEE Power and Energy Society Innovative Smart Grid Technologies Conference (ISGT)* (Washington, DC: IEEE), 1
- Panfilo, G., & Arias, F. 2019, *Metro*, 56, 42
- Perera, B., DeCesar, M., Demorest, P., et al. 2019, *MNRAS*, 490, 4666
- Petit, G., Thomas, C., & Tavella, P. 1993, *An ensemble pulsar time in 24th Annual Precise Time and Time Interval (PTTI) Applications and Planning Meeting* (Greenbelt, MA: NASA), 73-86
- Pizzocaro, M., Bregolin, F., & Barbieri, P. 2020, *Metro*, 57, 035
- Prasad, V., & Sharma, C. 2012, *Int. J. Eng. Technol.*, 2, 98
- Qiu, W., Yin, H., Zhang, L., et al. 2022, *IEEE T Smart Grid*, 13, 1654
- Rodin, A. 2008, *MNRAS*, 387, 1583
- Shaifullah, G. M., Magdalenic, J., Tiburzi, C., et al. 2022, *ASR*, 72, 5298
- Shen, D. 2018, Master thesis, National University of Defense Technology
- Tariq, I., Qiao, M., Wei, L., et al. 2022, *JINST*, 17, 03
- Yang, T., Gao, Y., Tong, M., et al. 2023, *Acta Aeronaut.*, 44, 526
- Yang, T., Tong, M., & Gao, Y. 2022, *RAA*, 22, 12
- Zhang, Y., Wang, Y., Yuan, H., et al. 2020, *Chin. Sci. Data*, 5, 11
- Zhou, Q., Wei, Z., Yan, L., et al. 2021a, *AcPSn*, 70, 139701
- Zhou, Q., Wei, Z., Zhang, H., et al. 2021b, *AcASn*, 62, 19